

Probing quantum chaos through singular-value correlations in sparse non-Hermitian SYK model

Pratik Nandy ^{1,2,*} Tanay Pathak ^{1,†} and Masaki Tezuka ^{3,‡}

¹*Center for Gravitational Physics and Quantum Information, Yukawa Institute for Theoretical Physics, Kyoto University, Kitashirakawa Oiwakecho, Sakyo-ku, Kyoto 606-8502, Japan*

²*RIKEN Interdisciplinary Theoretical and Mathematical Sciences Program (iTHEMS), Wako, Saitama 351-0198, Japan*

³*Department of Physics, Kyoto University, Kitashirakawa Oiwakecho, Sakyo-ku, Kyoto 606-8502, Japan*

Utilizing singular value decomposition, our investigation focuses on the spectrum of the singular values within a sparse non-Hermitian Sachdev-Ye-Kitaev (SYK) model. Unlike the complex eigenvalues typical of non-Hermitian systems, singular values are inherently real and positive. Our findings reveal a congruence between the statistics of singular values and those of the analogous Hermitian Gaussian ensembles. An increase in sparsity results in the non-Hermitian SYK model deviating from its chaotic behavior, a phenomenon precisely captured by the singular value ratios. Our analysis of the singular form factor (σ FF), analogous to the spectral form factor (SFF) indicates the disappearance of the linear ramp with increased sparsity. Additionally, we define singular complexity, inspired by the spectral complexity in Hermitian systems, whose saturation provides a critical threshold of sparseness. Such disintegration is likely associated with the breakdown of the existing holographic dual for non-Hermitian systems.

Introduction: Spectral statistics serve as a critical tool for probing the energy levels in quantum systems, offering insights into the dynamics within quantum chaos and Random Matrix Theory (RMT) [1–9]. Short-range statistics, encompassing level statistics, and the ratio of consecutive level spacings reveal the symmetries and randomness in the system [10]. Long-range correlations are captured by the Spectral Form Factor (SFF) [11–14], which in quantum chaotic systems, displays a dip-ramp-plateau structure [15]. It indicates the level-repulsion among the eigenvalues, a characteristic feature of quantum chaos [16] and has also been understood from the semiclassical gravity [17]. Recent investigations have yielded precise measurements of SFF, marking a significant advancement in probing quantum chaos in quantum many-body systems through experiments [18, 19].

Analogously, the upsurge in research has been directed towards unraveling the quantum chaotic properties of open quantum systems, primarily through the Lindbladian dynamics in RMT [20, 21] and operator growth, see [22] for a comprehensive review. These systems, interacting with external environments, are often described by non-Hermitian Hamiltonians [23–27], leading to complex eigenvalues. This connotes a departure from conventional methods suited for Hermitian systems and necessitates new methods for spectral analysis. Advances include generalizing level spacing ratios to complex planes [28] and adapting SFF to dissipative systems, known as Dissipative Spectral Form Factor (DSFF) [29–31], showing a quadratic ramp-plateau pattern diverging from the *linear* ramp structure seen in Hermitian systems. Several

other generalizations for SFF in non-Hermitian and open systems have also been proposed [32–34].

Recently, an alternative approach [35] considers the real and positive singular values of non-Hermitian Hamiltonians instead of the complex eigenvalues, obtained through Singular Value Decomposition (SVD) [36], as opposed to diagonalization. Aligning with the Hermitization process [37], this method facilitates a straightforward generalization of the frameworks used for Hermitian systems, bypassing the complexities associated with the complex plane. Such definitions have been fruitful in defining the singular spacing ratios [35] and singular form factor (σ FF) [38] in a much elegant manner that effectively captures the integrable to chaotic transitions, non-Hermitian many-body localization [38, 39] and non-Hermitian skin effect [40–42]. Outside this domain, SVD has also found applications in generalizing entanglement entropy for non-Hermitian transition matrices in AdS/CFT correspondence [43].

In this paper, we utilize the SVD framework to study the quantum chaotic properties and their transitions in the sparse, non-Hermitian version of the Sachdev-Ye-Kitaev (SYK) model [44, 45]. Standing as a quintessential archetype for quantum chaos and possessing a dual gravitational theory at low temperatures [46], the SYK model (see See [47, 48] for comprehensive reviews) can be adapted into sparse variants [49–53], maintaining its chaotic nature up to a critical sparsity threshold [54, 55]. This adaptation holds theoretical considerations in holography as well as the practical significance for the deployment of the SYK model on quantum processors [56, 57], where managing a sparse matrix is more viable. Our focus is particularly drawn to the influence that sparsity exerts on the average singular value spacing ratio,

* Authors' names are listed in alphabetical order.

denoted by $\langle r_\sigma \rangle$, and the σ FF, which serves as an extension of the conventional r -value [10] and the SFF in Hermitian systems, respectively. Additionally, we introduce *singular complexity*, inspired by spectral complexity, a boundary dual to the volume of the Einstein-Rosen bridge in gravitational theories [58]. Our findings suggest that these metrics proficiently encapsulate the transition from chaos to integrability in the non-Hermitian SYK model, as we outline in the following sections.

non-Hermitian SYK model: The prototypical model we consider is the 4-body non-Hermitian SYK model (nSYK), given by the following Hamiltonian [59, 60]

$$H_{\text{nSYK}} = \sum_{1 \leq a < b < c < d \leq N} (J_{abcd} + iM_{abcd}) \psi_a \psi_b \psi_c \psi_d, \quad (1)$$

where J_{abcd} and M_{abcd} are the independent random couplings drawn from the Gaussian ensemble with zero mean and variance $\langle J_{abcd}^2 \rangle = \langle M_{abcd}^2 \rangle = 6/N^3$. The variables ψ_k are the Majorana fermions obeying Clifford algebra $\{\psi_a, \psi_b\} = \delta_{ab}$. For numerical purposes, we consider the 4-body interactions only. The couplings M_{abcd} explicitly break the Hermiticity of the Hamiltonian (1), which otherwise reduces to the usual Hamiltonian [44, 45] when M_{abcd} vanishes for all $\{a, b, c, d\}$. This model has been pivotal in exploring non-Hermitian quantum chaos [61, 62].

In the following, we also consider the sparse version of the Hamiltonian (1), given by

$$H_{\text{nSYK}}^{\text{sparse}} = \sum_{1 \leq a < b < c < d \leq N} x_{abcd} (J_{abcd} + iM_{abcd}) \psi_a \psi_b \psi_c \psi_d. \quad (2)$$

In this sparse formulation, $x_{ijkl} \in [0, 1]$ are random variables that introduce an element of sparsity to the Hamiltonian. They follow a Gaussian distribution with zero mean and a variance of $\langle x_{abcd}^2 \rangle = 6/(pN^3)$ [49, 54]. The parameter p governs the probability of x_{abcd} being unity, thus determining the level of sparsity within the Hamiltonian. A fully *dense* model is characterized by $x_{abcd} = 1$ or $p = 1$ for all combinations of $\{a, b, c, d\}$, aligning with the original nSYK Hamiltonian (1). Conversely, a completely sparse model would have $x_{abcd} = 0$ or $p = 0$ for all combinations, representing the other extreme [49].

The probabilistic nature of x_{abcd} implies that the exact number of non-zero terms in $H_{\text{nSYK}}^{\text{sparse}}$ is not fixed but rather determined by the probability p . It is worth noting that one can choose to fix the number of non-zero terms in the sparse Hamiltonian (2) for each realization. However, such distinctions become less significant when considering the average over a large number of ensembles [54, 55]. For our study, we follow [55] without fixing the total number of terms in the sparse Hamiltonian in each realization.

Singular value decomposition and singular value statistics: In Hermitian systems, the eigenspectrum of the

Hamiltonian is a key indicator of chaotic dynamics. The eigenvalues E_n are real, allowing for the definition of consecutive level spacings $s_n = E_{n+1} - E_n$, as an ordered list. For large Hilbert spaces, the average consecutive level spacing ratio r_n is defined as $r_n = \min(s_n, s_{n+1})/\max(s_n, s_{n+1})$ with $\langle r \rangle = \text{mean}(r_n)$ being the *average r value* [10]. Its usefulness lies in the simplification of the numerical analysis by bypassing the need to unfold the spectrum for level statistics. Typically, the r -ratio statistics is derived from the mid-spectrum, avoiding edge anomalies. For Gaussian Orthogonal Ensemble (GOE), Gaussian Unitary Ensemble (GUE), and Gaussian Symplectic Ensemble (GSE), the level statistics follow the Wigner-Dyson distribution with an average $\langle r \rangle_{\text{GOE}} \approx 0.53590$, $\langle r \rangle_{\text{GUE}} \approx 0.60266$ and $\langle r \rangle_{\text{GSE}} \approx 0.67617$ respectively while the Poissonian distribution corresponds to $\langle r \rangle_{\text{P}} \approx 0.386$ [10]. It is important to note that these values (except for $\langle r \rangle_{\text{P}}$) are for three-dimensional matrices, and they decrease as the dimension increases. Numerically such values can be obtained by fitting the data at appropriate matrix dimensions [10].

While $\langle r \rangle$ -value is well-defined for Hermitian systems, it falls short in applying for non-Hermitian systems where eigenvalues are complex, and thus an ordered sequence of level spacings is not feasible. In such scenarios, one must consider complex spacing ratios [28], which are defined in the two-dimensional complex plane. Consequently, the consecutive level spacings are generalized to the Euclidean distance between the eigenvalues in the complex plane, and the complex spacing ratio is then defined by taking the ratio of the distance from a given eigenvalue to its nearest neighbor, to the distance to its second nearest neighbor. However, this definition does not reduce to $\langle r \rangle$ -value for Hermitian systems. Rather it reduces to a different $\langle r \rangle$ -value formed by the closest and second closest neighbors from the ordered set [63].

In a recent work [35], an alternate proposal was suggested. Instead of focusing on complex eigenvalues, the analysis is based on singular values derived from the singular value decomposition (SVD) of the Hamiltonian. SVD is expressed as $H = U \Sigma V^\dagger$, where U and V are $N \times N$ unitary matrices satisfying $U^\dagger U = V^\dagger V = 1$, and $\Sigma = \text{diag}(\sigma_1, \dots, \sigma_N)$ is a diagonal matrix containing the singular values σ_i . Singular values are always positive and applicable to both Hermitian and non-Hermitian matrices. For Hermitian matrices, singular values reduce to the absolute values of the eigenvalues, but for non-Hermitian matrices, the singular values and eigenvalues are not straightforwardly related [64]. Importantly, the techniques of SVD are advantageous over other methods such as bi-orthogonalization, where the Hamiltonian can be diagonalized by a bi-orthogonal transformation such that $H = P \Lambda Q^\dagger$, where $\Lambda = \text{diag}(E_1, \dots, E_n)$ is a diagonal matrix containing the complex eigenvalues of the non-Hermitian Hamiltonian [65]. The matrices P and Q are not individually unitary, but they are bi-unitary

System	$N = 20$	$N = 22$	$N = 24$	$N = 26$	$N = 28$	$N = 30$
$\langle r \rangle_{\text{RMT}}$	0.6744	0.5996	0.5307	0.5996	0.6744	0.5996
$\langle r \rangle_{\text{nSYK}}$	0.6744	0.5997	0.5307	0.5996	0.6745	0.5995

TABLE I. The Table shows the $\langle r_\sigma \rangle$ -values for the non-Hermitian SYK model (1) for different system sizes $N = 20$ (10000), $N = 22$ (6000), $N = 24$ (2000), $N = 26$ (1000), $N = 28$ (100), and $N = 30$ (50), where the parenthesis includes the number of samples taken. Here $N \bmod 8 = 0$ (GOE), 2, 6 (GUE), and 4 (GSE) [68]. The values are in precise agreement (with numerical accuracy) with the $\langle r \rangle_{\text{RMT}}$ -values for large N results given in [10].

satisfying $P^\dagger Q = Q^\dagger P = 1$.

SVD is a fundamental matrix factorization technique in linear algebra [36]. Curiously, the singular values of a non-Hermitian matrix H can be computed without directly performing SVD. This method, known as *Hermitization* [37], involves constructing a new matrix \mathbf{H} , twice the dimension of H . This larger matrix incorporates both H and its Hermitian conjugate H^\dagger in a block structure. The matrix \mathbf{H} is defined as [37]

$$\mathbf{H} = \begin{pmatrix} \mathbf{0} & H \\ H^\dagger & \mathbf{0} \end{pmatrix} \Rightarrow \mathbf{H}^2 = \begin{pmatrix} HH^\dagger & \mathbf{0} \\ \mathbf{0} & H^\dagger H \end{pmatrix}. \quad (3)$$

The eigenvalues of \mathbf{H} are $\{\pm\sigma_n\}$, precisely containing the singular values of H . This is because the non-zero blocks in \mathbf{H} are off-diagonal, leading to a characteristic polynomial that yields the squares of the singular values of H as eigenvalues. This is equivalent to constructing an effective Hamiltonian H_{eff} , by taking the square root of the product H and H^\dagger such that $H_{\text{eff}} = \sqrt{H^\dagger H}$ or $H_{\text{eff}} = \sqrt{H H^\dagger}$. The eigenvalues of H_{eff} represent the singular values of H [37]. Such construction of a Hermitized matrix resembles the formulation of the Wishart SYK model and its supersymmetric version, comprised of non-Hermitian conserved charges or supercharges [66, 67].

Given the singular values $\{\sigma_i\}$ of the corresponding non-Hermitian Hamiltonian H , one analogously defines $\lambda_i = \sigma_{i+1} - \sigma_i$ as the *singular value spacings*. Consequently, the *singular-value-spacing ratio* r_σ is defined analogous to the r -ratio as [35]

$$r_{\sigma,n} = \frac{\min(\lambda_i, \lambda_{i+1})}{\max(\lambda_i, \lambda_{i+1})}, \quad \langle r_\sigma \rangle = \text{mean}(r_{\sigma,n}). \quad (4)$$

Referred to as the *average r_σ value*, these values adhere to statistical distributions akin to those observed for non-Hermitian Hamiltonians, similar to the $\langle r \rangle$ -value distributions for Hermitian matrices. This framework has been instrumental in the 38-fold symmetry classification in non-Hermitian systems [35].

Table I showcases the $\langle r_\sigma \rangle$ -value for the dense non-Hermitian SYK model (1) for varying system sizes N , representing the total number of fermions. The data is juxtaposed with corresponding Hermitian Gaussian

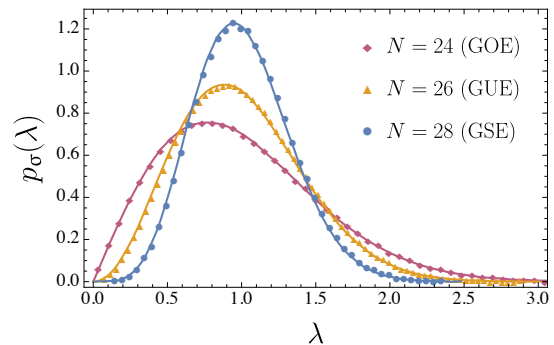


FIG. 1. The consecutive singular level-spacing distribution in the non-Hermitian dense SYK model (1) for $N = 24$ (2000) (GOE), $N = 26$ (1000) (GUE) and $N = 28$ (100) (GSE) with the corresponding realizations shown in the brackets. The solid lines represent distribution for GOE, GUE, and GSE respectively taking matrices of size $10^4 \times 10^4$ with averaging over 1000 realizations.

ensembles, revealing a striking correlation that underscores the utility of the $\langle r_\sigma \rangle$ -value in understanding non-Hermitian systems. Figure 1 correspondingly shows the consecutive *singular level-spacing distribution* $p_\sigma(\lambda)$ for $N = 24$ (GOE), $N = 26$ (GUE) and $N = 28$ (GSE) respectively, which are *approximated* by the Wigner-Dyson distribution [1]

$$p(\lambda) = \begin{cases} \frac{\pi\lambda}{2} e^{-\frac{\pi\lambda^2}{4}} & \text{GOE,} \\ \frac{32\lambda^2}{\pi^2} e^{-\frac{4\lambda^2}{\pi}} & \text{GUE,} \\ \left(\frac{64}{9\pi}\right)^3 e^{-\frac{64\lambda^2}{9\pi}} & \text{GSE.} \end{cases} \quad (5)$$

with the normalization $\int_0^\infty p(\lambda)d\lambda = \int_0^\infty \lambda p(\lambda)d\lambda = 1$.

SVD in sparse non-Hermitian SYK model: In the preceding discussion, we delved into the behavior of the r_σ -ratio for the non-Hermitian SYK model, given by equation (1), across various system sizes. We now turn our attention to the sparse variant of this model, which is governed by the sparsity parameter p . Our aim is to elucidate the impact of sparsity on the $\langle r_\sigma \rangle$ -ratio during the transition from a densely connected to a sparsely connected regime.

Figure 2 illustrates how the average $\langle r_\sigma \rangle$ -value varies with the sparsity parameter p for different system sizes. Each system size, representing a distinct ensemble, is depicted in a unique color. The dotted lines mark the expected values for Poisson statistics and the Hermitian ensemble, as specified in Table I. It is observed that the Hamiltonian (2) retains its chaotic nature up to a critical level of sparsity denoted by p_{crit} . This chaotic behavior is also corroborated by the $\langle r \rangle$ -ratio presented in Table I. Consequently, we define a transition point p_{crit} beyond which the Hamiltonian (2) ceases to exhibit chaotic dynamics. Such transition point is obtained by considering approximately 99% of the corresponding $\langle r_\sigma \rangle$ value at $p = 1$ [55]. Notably, as the system size increases, this

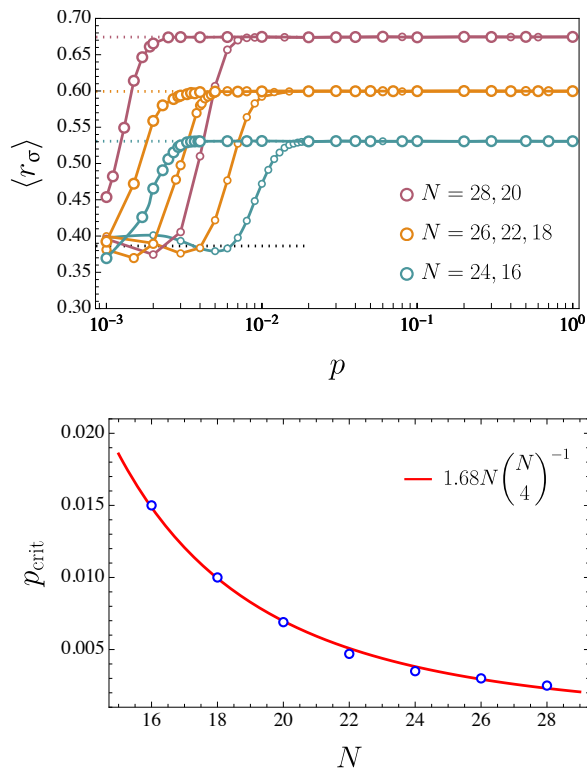


FIG. 2. (Top) Variation of $\langle r_\sigma \rangle$ -value with various level of sparsity p . The size of the circle varies with N i.e., the largest N corresponds to the leftmost plot for each color. At low sparsity, the $\langle r_\sigma \rangle$ matches with the corresponding random matrix ensemble until a threshold p_{crit} is reached, after which $\langle r_\sigma \rangle$ drops to the Poissonian value, indicating a hint of integrability. The estimated errors for the values obtained is smaller than the markers in the plot. (Bottom) The finite-size dependence of the threshold or the critical value p_{crit} . It decreases as the system size increases. The decrease is $1/N^3$ with a large system size, as given in (6).

transition point migrates towards lower sparsity levels. When the sparsity is sufficiently low, the $\langle r_\sigma \rangle$ -value aligns with the Poisson limit, signifying the Hamiltonian's transition to integrability.

In conjunction with the above, we also present the relationship between the critical sparsity p_{crit} and the system size N . Intriguingly, the critical value diminishes as the system size increases. This reduction follows a power-law trend, best described by fitting the data to the curve [55]

$$p = kN \binom{N}{4}^{-1} \approx \frac{24k}{N^3}, \quad (6)$$

in the large N limit. where the decrease is proportional to $1/N^3$ and the constant k is approximately 1.68, as determined by the fitting process. This scaling behavior is consistent with that observed for the sparse Hermitian SYK model, as reported in [54, 55].

Spectral and Singular form factor: In the realm of quantum chaos, the Spectral Form Factor (SFF) serves as

a pivotal tool for probing the full spectrum of eigenvalue correlations, encompassing both short and long-range interactions. The SFF is defined as the Fourier transform of two-point eigenvalue correlation pairs [12–14]

$$\text{SFF}(t) = \frac{1}{L^2} \langle |Z_E(it)|^2 \rangle = \frac{1}{L^2} \left\langle \left| \sum_n e^{-iE_n t} \right|^2 \right\rangle, \quad (7)$$

where $Z_E(it) = \sum_n e^{-iE_n t}$ is the infinite-temperature partition function for the energy eigenvalues, and L is the dimension of the Hilbert space. Here the angle brackets indicate an ensemble average, which is particularly relevant in the context of a disordered system since SFF is not self-averaging [69]. Throughout our discussion, we consider the *quenched* disorder, instead of *annealed* one, which is less physical in this scenario. Interestingly, in the context of a disorder-free SYK model [70], the SFF reveals indications of integrability, marking a departure from the chaotic behavior [71].

For systems exhibiting quantum chaos, the SFF displays a characteristic dip-ramp-plateau pattern. The initial dip, evident in the early-time regime, is a non-universal trait influenced by the detailed nature of the energy spectrum [11]. This dip extends until a timescale known as the *Thouless time* (t_{Th}) [72, 73] or *ramp time* [16] beyond which the energy difference surpasses the inverse of (t_{Th}), referred to as the *Thouless energy* [74]. Subsequently, a ramp emerges at t_{Th} , indicative of eigenvalue repulsion, a phenomenon that mirrors the SFF behavior predicted by RMT [14, 16] and underscores the chaotic dynamics of the Hamiltonian. Moreover, this ramp hints at the presence of a holographic dual to the corresponding theory. Beyond the *Heisenberg time* [69, 75], which scales inversely to the mean level spacing, the SFF reaches a plateau that depends on the system size. In contrast, integrable systems typically bypass the ramp stage and saturate directly from the dip to the plateau regime. SFF in sparse SYK models has been thoroughly investigated in the literature [50, 51, 54, 55].

Analogous to the SFF, the singular form factor (σFF) is defined as [38]

$$\sigma\text{FF}(t) = \frac{1}{L^2} \langle |Z_\sigma(it)|^2 \rangle = \frac{1}{L^2} \left\langle \left| \sum_n e^{-i\sigma_n t} \right|^2 \right\rangle, \quad (8)$$

where $Z_\sigma(it) = \sum_n e^{-i\sigma_n t}$ is the infinite-temperature partition function of singular values, which can be further expressed as the overlap between the time-evolved right or left singular vectors governed by the effective Hamiltonian $\sqrt{H^\dagger H}$ or $\sqrt{H H^\dagger}$ respectively [38].

Figure 3 shows the distinct dip-ramp-plateau pattern exhibited by σFF for the non-Hermitian model (2), across varying degrees of sparsity. In this study, we consider a system size of $N = 26$ and analyze the outcomes from 1000 independent realizations of the Hamiltonian to ensure robust statistical analysis. To reduce the oscillations

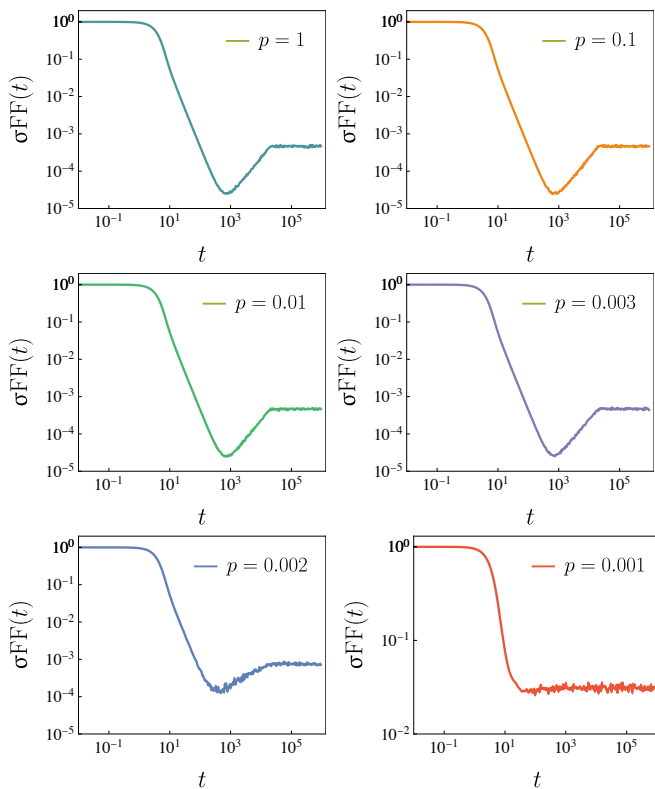


FIG. 3. Behavior singular form factor $\sigma\text{FF}(t)$ for various sparseness parameter p . The linear ramp ceases to exist as the sparseness increases. The system parameters are $N = 26$ (GUE) with 1000 Hamiltonian realizations. Here we choose the Gaussian filter (10) with $\alpha = 3.27$, which lies within the prescribed range in [55].

in the dip region, we use the filter function $Y_\sigma(\alpha, t)$ [72] such that

$$\sigma\text{FF}(t) = \left\langle \frac{|Y_\sigma(\alpha, t)|^2}{|Y_\sigma(\alpha, 0)|^2} \right\rangle, \quad (9)$$

Here the filter function for the singular values is chosen to be Gaussian, which we refer to as the Gaussian *singular* filter function. It is defined as

$$|Y_\sigma(\alpha, t)|^2 = \left| \sum_n e^{-\alpha\sigma_n^2} e^{-i\sigma_n t} \right|^2. \quad (10)$$

As shown for Hermitian systems, given the energy spectrum is centered around $E = 0$, such a filter function modifies the density of states $\rho(E) \rightarrow e^{-\alpha E^2} \rho(E)$ such that the σFF receives the dominant contribution from the bulk of the energy spectrum [72, 73]. Here α is a free parameter and controls the Gaussianity of the spectrum. This filtering avoids the unfolding which can otherwise be studied using the *connected unfolded* SFF [73]. For our computation, we employ the filter function on the singular values by choosing $\alpha = 3.27$, which lies inside the range given in [55] (dependent on N). Filter functions

for SFF have also recently been shown to be associated with quantum channels [76].

A notable observation is a parallelism between the behavior of σFF in non-Hermitian systems and the SFF in Hermitian systems. This similarity underscores the efficacy of σFF as a robust indicator for quantum chaos in non-Hermitian frameworks. In regimes of lower sparsity, the presence of the ramp is clearly evident, signifying the retention of chaotic dynamics within this parameter space. It remains pronounced until a critical sparsity threshold is reached. Beyond this juncture, the linear ramp—a signature trait of non-integrable systems—ceases to manifest, indicating a shift towards regularity and a departure from chaotic behavior.

Figure 4 shows the variation of Thouless time (t_{Th}), for $N = 26$, with sparseness parameter p . The t_{Th} is calculated by considering the time at which the σFF of the system considered first intersects the SFF of the GUE random matrices [16]. To determine the intersection point precisely we consider the the following fractional error function [72]

$$\epsilon(t) := \left| \frac{\sigma\text{FF}(t) - \sigma_{\text{ramp}}(t)}{\sigma_{\text{ramp}}(t)} \right|, \quad (11)$$

indicating the deviation of the computed σFF to the linear-fitted function for the ramp $\sigma_{\text{ramp}}(t)$ for $p = 1$ (dense SYK model (1)). We consider the value t as the Thouless time or ramp time t_{Th} , where the fractional error $\epsilon(t)$ reaches 20%. The red line shows the fitting $t_{\text{Th}} \approx a/p^b + c$ with $a = 1.923$, $b = 0.8767$ and $c = 0.007$. Curiously, this fitting follows closely to the $1/p$ scaling in contrast to the $1/p^2$ scaling in Hermitian systems [55]. Such distinction is possible since the singular values and the eigenvalues are inherently different. Yet, we do not rule out the possibility of the scaling of the exponent b with the system size.

In Hermitian systems, a key observation is that the singular values correspond to the absolute values of the eigenvalues. This distinction is crucial, as it implies that the SFF and σFF , exhibit fundamentally different behaviors. This difference is illustrated in the inset of Fig. 4, which depicts the dynamics of SFF and σFF for the dense Hermitian SYK₄ model. The model is derived by setting $M_{abcd} = 0$ for all $\{a, b, c, d\}$ in its non-Hermitian counterpart (Eq. (1)). Replacing σ_n by eigenvalues E_n in (9), we get the analogous definition of filtered SFF.

Notably, the singular values offer a *weaker* effect compared to the eigenvalues, considering the ramp. However, to reduce the SFF from σFF , we consider the following prescription. From SVD, we obtain two sets of vectors, the left and right singular vectors. They are related by

$$H |u_n\rangle = \sigma_n |v_n\rangle, \quad H^\dagger |v_n\rangle = \sigma_n |u_n\rangle, \quad (12)$$

where $\{\sigma_n\}$ are the singular values. For Hermitian systems, the eigenvalues are real, and the left ($|u_n\rangle$) and the

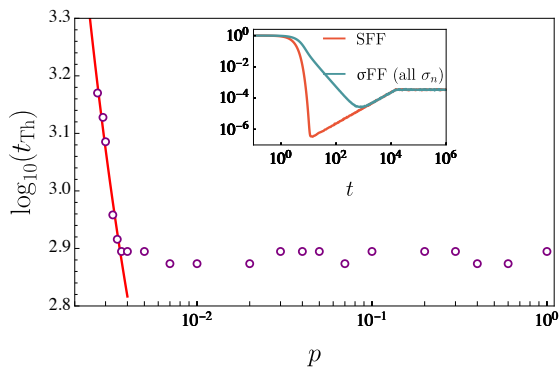


FIG. 4. (Main plot) Thouless time (ramp time) with respect to sparsity parameter. The red line is the fit $t_{\text{Th}} \approx a/p^b + c$ with $a = 1.923$, $b = 0.8767$ and $c = 0.007$. (Inset) The behavior of SFF and the σFF for the Hermitian dense SYK₄ model. The system parameters are $N = 26$ with 1000 random Hamiltonian realizations taken. The σFF (green line) is computed considering all the positive singular values. It reduces to the SFF after taking the appropriate rescaling of the singular vectors and singular values, which otherwise equals the eigenvalues (with appropriate signs).

System	$\langle r_\sigma \rangle$	$\langle r \rangle$	$\langle r_+ \rangle$	$\langle r_- \rangle$	$\langle r \rangle$ (2 blocks)
nSYK ($N = 20$)	0.4119	0.6743	0.6744	0.6744	0.4117
nSYK ($N = 22$)	0.4220	0.5994	0.5998	0.5991	0.4220
nSYK ($N = 24$)	0.4238	0.5303	0.5303	0.5302	0.4234

TABLE II. The Table shows the comparison between the singular value $\langle r_\sigma \rangle$ -value and the $\langle r \rangle$ -values for the *dense* Hermitian SYK model for different system sizes $N = 20$ (GSE), $N = 22$ (GUE), $N = 24$ (GOE). We take 1000 Hamiltonian realizations for each case. The Hermitian model is obtained by setting $M_{abcd} = 0$ for all $\{a, b, c, d\}$ in (1). Here the $\langle r_+ \rangle$ -value includes the positive eigenvalues while $\langle r_- \rangle$ -value includes the negative eigenvalues only. They are to be matched with the $\langle r \rangle_{\text{RMT}}$ values in Table I and [10]. The $\langle r_\sigma \rangle$ -values are compared with the $\langle r \rangle$ -value of 2 blocks (marked in blue) [55]. Explanation is given in the text.

right ($|v_n\rangle$) singular vectors are related with a factor of ± 1 . If the left and right singular vectors are equal, i.e., $|u_n\rangle = |v_n\rangle$ for some n , then the corresponding singular value exactly equals the eigenvalue i.e., $\sigma_n = E_n$. However, if they differ by a negative sign i.e., $|u_n\rangle = -|v_n\rangle$ for some n , then the corresponding singular value and the eigenvalue differs by a negative sign i.e., $\sigma_n = -E_n$. It is thus straightforward to identify such vectors such that the singular values can be directly mapped with the eigenvalues, and correspondingly compute the σFF . In this case, the σFF exactly equals the SFF as shown by the red line in the inset of Fig. 4.

Intriguingly, the Hermitian system exhibits a unique characteristic in its $\langle r_\sigma \rangle$ -value as well. As depicted in Table II, there is a notable distinction when comparing the $\langle r_\sigma \rangle$ -value to the $\langle r \rangle$ -values within the identical Hermitian SYK₄ model. Additionally, the $\langle r_+ \rangle$ -value and

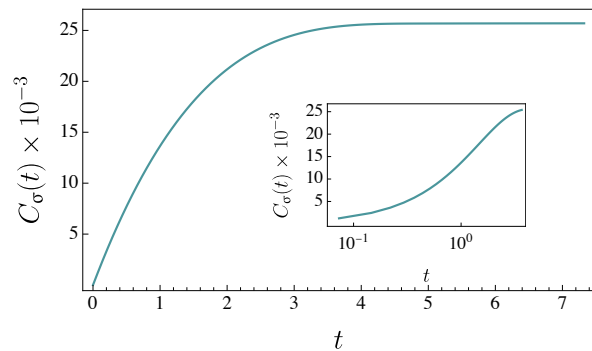


FIG. 5. Behaviour of the singular complexity with time for dense ($p = 1$) non-Hermitian SYK model (1). The system parameter is $N = 26$ with 1000 random Hamiltonian realizations taken. Inset shows the early time behavior of the complexity, which increases quadratically followed by linear growth and saturation.

$\langle r_- \rangle$ -value were computed separately, considering only the positive and negative eigenvalues of the Hamiltonian, respectively. These ratios align with the overall $\langle r \rangle$ -value, which is anticipated since it solely accounts for the spacing between consecutive eigenvalues. Nonetheless, these individual ratios as well as the overall $\langle r \rangle$ -value do not correspond to the $\langle r_\sigma \rangle$ -value, which is identified as the $\langle r \rangle$ -value for two separate blocks before symmetry resolution. This discrepancy arises because, in Hermitian systems, the singular values are determined by the absolute magnitudes of the eigenvalues, leading to the computation of the $\langle r_\sigma \rangle$ -value mirroring the $\langle r \rangle$ -value for bifurcated blocks [35, 55, 77]. We anticipate such bifurcation has a similar effect of having the presence of conserved charges [66, 67]. Curiously, this phenomenon is exclusive to Hermitian and anti-Hermitian (with $J_{abcd} = 0$, $M_{abcd} \neq 0$) systems and echoes the discrepancy between the σFF and SFF as shown in the inset of Fig. 4.

It is imperative to differentiate the behavior of σFF from the dissipative spectral form factor (DSFF), especially since DSFF has been instrumental in deciphering chaos in non-Hermitian and open systems [29–31]. The σFF is characterized by its reliance on real singular values, whereas the DSFF encompasses the complex eigenspectrum, establishing a fundamental difference between the two. The DSFF reveals a unique quadratic ramp-plateau structure in non-Hermitian systems [29, 30]. Meanwhile, the σFF , while also mirroring the SFF exactly for Hermitian systems upon the appropriate identification of the singular vectors, preserves the linear ramp-plateau configuration. It, thus, serves as an effective marker for the transition between integrable and chaotic phases. Therefore, despite their inherent differences, both metrics are apt for exploring the nuances of non-Hermitian and open quantum systems.

Spectral complexity for singular values - Singular complexity: A related quantity, capturing the long-range

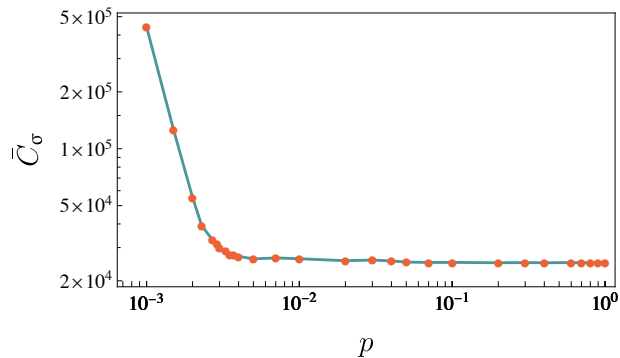


FIG. 6. Behaviour of the saturation of the singular complexity with different sparseness for $N = 26$ with 1000 random Hamiltonian realizations.

spectral correlation is motivated by considering the spectral complexity [58]. Within the framework of the AdS/CFT duality [78, 79], spectral complexity finds its counterpart in the volumetric measure of the Einstein-Rosen bridge, serving as an analog for the computational and circuit complexity [80]. In a similar spirit, we define *singular complexity* at finite temperature $T = 1/\beta$ as

$$C_{\sigma}(t) = \frac{1}{Z_{2\sigma}(\beta)L} \sum_{\sigma_i \neq \sigma_j} \left[\frac{\sin(t(\sigma_i - \sigma_j)/2)}{(\sigma_i - \sigma_j)/2} \right]^2 e^{-\beta(\sigma_i + \sigma_j)}, \quad (13)$$

designed to be suitable for non-Hermitian systems. Here $Z_{\sigma}(\beta) = \sum_n e^{-\beta\sigma_n}$ is the thermal *singular partition function*, constructed from the singular values of the corresponding non-Hermitian Hamiltonian. Assuming no degeneracy in the singular value spectrum, the derivative of the singular complexity is related to the σ FF as

$$\frac{d^2}{dt^2} C_{\sigma}(t) = \frac{2}{L} \frac{Z_{\sigma}(\beta)^2}{Z_{\sigma}(2\beta)} \sigma\text{FF}(t) - \frac{2}{L}, \quad (14)$$

in a similar spirit to spectral complexity [58, 81] which can be checked directly using (8). Focusing on the infinite temperature $\beta = 0$ limit, (13) takes a simpler form

$$C_{\sigma}(t) = \frac{1}{L^2} \sum_{\sigma_i \neq \sigma_j} \left[\frac{\sin(t(\sigma_i - \sigma_j)/2)}{(\sigma_i - \sigma_j)/2} \right]^2. \quad (15)$$

At early times, it grows quadratically as $C_{\sigma}(t) \approx (1 - \frac{1}{L})t^2$, followed by a linear growth and plateau regime. The plateau value can be obtained analytically by taking the long-time average

$$\bar{C}_{\sigma} = \lim_{t_f \rightarrow \infty} \frac{1}{t_f} \int_0^{t_f} C_{\sigma}(t) dt = \frac{2}{L^2} \sum_{\sigma_i \neq \sigma_j} \frac{1}{(\sigma_i - \sigma_j)^2}, \quad (16)$$

which only depends on the difference between the singular values. For the eigenvalues, such saturation values have been studied for quantum billiards [82] and

mixed-field Ising model [83], capturing the *spectral rigidity*. Integrable systems tend to saturate at higher values compared to the chaotic ones due to the presence of level-repulsion which directly affects the equivalent eigen-spectrum of (16). At early times, the relation between spectral complexity and spread complexity [84] based on Krylov space approach [85] in the Hermitian settings has also been proposed [81]; see [22] for a detailed discussion.

Figure 5 shows the time evolution of the infinite-temperature singular complexity (15) for the dense Hamiltonian (1) with $N = 26$ and 1000 realizations. The complexity grows quadratically, followed by linear growth (inset) and saturation. Correspondingly, Fig. 6 depicts how the singular complexity approaches saturation at varying levels of sparsity, maintaining a magnitude order of $O(10^4)$ until it encounters a critical threshold. Beyond this threshold, there is a marked escalation at lower sparsity levels signaling an analogous level-repulsion between the singular values. This critical value is dependent on the system size N , and for $N = 26$, it occurs within the sparsity regime $0.003 \lesssim p_{\text{crit}} \lesssim 0.004$. This value resembles the expected $\langle r_{\sigma} \rangle$ -ratio shown in Fig. 2.

Exhibiting chaotic dynamics is considered to be a crucial constraint that possesses a holographic dual geometry. While this discussion does not explore the specifics of such geometry, some proposals exist in the literature [59, 86, 87]. The breakdown of chaotic nature suggests that such dual geometry corresponding to a non-Hermitian system may be compromised at low sparsity.

Conclusion and Outlook: Drawing on the foundational work [35] on the applicability of SVD in non-Hermitian systems, our study delves into the quantum chaotic attributes of the sparse SYK model across varying levels of sparsity. The complex eigenvalues inherent to non-Hermitian Hamiltonians pose challenges to the generalization of traditional eigenvalue statistics. This complexity persists despite strides made with complex spacing ratios [28] and the DSFF [29, 30]. Nonetheless, recent advancements propose a novel perspective by focusing on singular values as opposed to eigenvalues within the non-Hermitian framework. Unlike their complex counterparts, singular values are inherently real and positive, aligning with the real eigenvalues in Hermitian systems upon appropriate alignment with singular vectors, as detailed in the main text.

Our investigation underscores that the statistical analysis of singular values, which elucidates short-range correlations, coupled with the σ FF and singular complexity, illuminating long-range correlations among singular values, serve as potent indicators of the chaos within non-Hermitian systems. As such, exploring the holographic bulk dual of singular complexity may offer insights into a potential holographic counterpart for non-Hermitian systems, especially the effective range of k in (6) in relation to $2d$ de Sitter (dS_2) gravity [86], which we leave for future work. Moreover, these tools adeptly re-

flect the shift towards integrability as sparsity intensifies. Notably, such transition is different than other chaotic-integrable transitions by two-point interactions observed in the SYK model [88]. We envision that these features will be exhibited in other correlation measures such as higher spacing ratios [63, 89] and the number variance [32, 72, 90, 91].

Parallel research avenues have explored the efficacy of sparse Hamiltonians [49, 50] within quantum processors [56, 57], maintaining chaotic dynamics to a substantial degree of sparsity. Notably, the SYK model retains its holographic duality even at minimal sparsity levels [54, 55]. Our study contributes to the burgeoning field of non-Hermitian systems and open-system dynamics, proposing a framework for the extrapolation of quantum chaotic properties within these systems. This might serve as the benchmark results for the simulation of sparse non-Hermitian systems on quantum processors.

Acknowledgements: We would like to thank Hugo A. Camargo, Adolfo del Campo, Antonio M. García-García, Luca V. Iliesiu, Hosho Katsura, and Tadashi Takayanagi for fruitful discussions, comments, and suggestions on the draft. Numerical calculations were performed in the *Sushiki* workstation using the computational facilities of YITP. P.N. thanks the Berkeley Center for Theoretical Physics (BCTP), University of California for hosting him through the Adopting Sustainable Partnerships for Innovative Research Ecosystem (ASPIRE) program of Japan Science and Technology Agency (JST), Grant No. JPM-JAP2318 during the final stages of the work. This work is supported by the Japan Society for the Promotion of Science (JSPS) Grants-in-Aid for Transformative Research Areas (A) “Extreme Universe” No. JP21H05190 (P.N.) and JP21H05182, JP21H05185 (M.T.). The Yukawa Research Fellowship of T.P. is supported by the Yukawa Memorial Foundation and JST CREST (Grant No. JPMJCR19T2). The work of M.T. was partially supported by the JSPS Grants-in-Aid for Scientific Research (KAKENHI) Grants No. JP20K03787.

* pratik@yukawa.kyoto-u.ac.jp

† pathak.tanay@yukawa.kyoto-u.ac.jp

‡ tezuka@scphys.kyoto-u.ac.jp

- [1] M.L. Mehta, *Random Matrices* (Academic Press, 1991).
- [2] O. Bohigas, M. J. Giannoni, and C. Schmit, “Characterization of chaotic quantum spectra and universality of level fluctuation laws,” *Phys. Rev. Lett.* **52**, 1–4 (1984).
- [3] Eugene P. Wigner, “Characteristic Vectors of Bordered Matrices With Infinite Dimensions,” *Annals of Mathematics* **62**, 548–564 (1955).
- [4] Eugene P. Wigner, “Characteristics Vectors of Bordered Matrices with Infinite Dimensions II,” *Annals of Mathematics* **65**, 203–207 (1957).
- [5] Freeman J. Dyson, “Statistical Theory of the Energy Levels of Complex Systems. I,” *Journal of Mathematical Physics* **3**, 140–156 (1962).
- [6] Freeman J. Dyson, “Statistical Theory of the Energy Levels of Complex Systems. II,” *Journal of Mathematical Physics* **3**, 157–165 (1962).
- [7] Freeman J. Dyson and Madan Lal Mehta, “Statistical Theory of the Energy Levels of Complex Systems. IV,” *Journal of Mathematical Physics* **4**, 701–712 (1963).
- [8] Michael Victor Berry, M. Tabor, and John Michael Ziman, “Level clustering in the regular spectrum,” *Proceedings of the Royal Society of London. A. Mathematical and Physical Sciences* **356**, 375–394 (1977).
- [9] M. V. Berry and M. Tabor, “Closed orbits and the regular bound spectrum,” *Proceedings of the Royal Society of London. Series A, Mathematical and Physical Sciences* **349**, 101–123 (1976).
- [10] Y. Y. Atas, E. Bogomolny, O. Giraud, and G. Roux, “Distribution of the ratio of consecutive level spacings in random matrix ensembles,” *Phys. Rev. Lett.* **110**, 084101 (2013).
- [11] Oded Agam, Boris L. Altshuler, and Anton V. Andreev, “Spectral statistics: From disordered to chaotic systems,” *Phys. Rev. Lett.* **75**, 4389–4392 (1995).
- [12] Luc Leviandier, Maurice Lombardi, Rémi Jost, and Jean Paul Pique, “Fourier transform: A tool to measure statistical level properties in very complex spectra,” *Phys. Rev. Lett.* **56**, 2449–2452 (1986).
- [13] Joshua Wilkie and Paul Brumer, “Time-dependent manifestations of quantum chaos,” *Phys. Rev. Lett.* **67**, 1185–1188 (1991).
- [14] E. Brézin and S. Hikami, “Spectral form factor in a random matrix theory,” *Phys. Rev. E* **55**, 4067–4083 (1997).
- [15] Thomas Guhr, Axel Muller-Groeling, and Hans A. Weidenmuller, “Random matrix theories in quantum physics: Common concepts,” *Phys. Rept.* **299**, 189–425 (1998).
- [16] Jordan S. Cotler, Guy Gur-Ari, Masanori Hanada, Joseph Polchinski, Phil Saad, Stephen H. Shenker, Douglas Stanford, Alexandre Streicher, and Masaki Tezuka, “Black Holes and Random Matrices,” *JHEP* **05**, 118 (2017), [Erratum: *JHEP* 09, 002 (2018)].
- [17] Phil Saad, Stephen H. Shenker, and Douglas Stanford, “A semiclassical ramp in SYK and in gravity,” (2018), [arXiv:1806.06840 \[hep-th\]](https://arxiv.org/abs/1806.06840).
- [18] Adway Kumar Das *et al.*, “Proposal for many-body quantum chaos detection,” (2024), [arXiv:2401.01401 \[cond-mat.stat-mech\]](https://arxiv.org/abs/2401.01401).
- [19] Hang Dong *et al.*, “Measuring Spectral Form Factor in Many-Body Chaotic and Localized Phases of Quantum Processors,” (2024), [arXiv:2403.16935 \[quant-ph\]](https://arxiv.org/abs/2403.16935).
- [20] Sergey Denisov, Tetyana Laptyeva, Wojciech Tarnowski, Dariusz Chruściński, and Karol Życzkowski, “Universal spectra of random Lindblad operators,” *Phys. Rev. Lett.* **123**, 140403 (2019).
- [21] Yifeng Yang, Zhenyu Xu, and Adolfo del Campo, “Decoherence rate in random Lindblad dynamics,” *Phys. Rev. Res.* **6**, 023229 (2024).
- [22] Pratik Nandy, Apollonas S. Matsoukas-Roubeas, Pablo Martínez-Azcona, Anatoly Dymarsky, and Adolfo del Campo, “Quantum Dynamics in Krylov Space: Methods and Applications,” (2024), [arXiv:2405.09628 \[quant-ph\]](https://arxiv.org/abs/2405.09628).
- [23] Carl M. Bender and Stefan Boettcher, “Real spectra in nonHermitian Hamiltonians having PT symmetry,” *Phys. Rev. Lett.* **80**, 5243–5246 (1998).
- [24] Naoyuki Shibata and Hosho Katsura, “Dissipative spin

- chain as a non-Hermitian Kitaev ladder,” *Phys. Rev. B* **99**, 174303 (2019).
- [25] Yuto Ashida, Zongping Gong, and Masahito Ueda, “Non-Hermitian physics,” *Adv. Phys.* **69**, 249–435 (2021).
- [26] Julien Cornelius, Zhenyu Xu, Avadh Saxena, Aurelia Chenu, and Adolfo del Campo, “Spectral Filtering Induced by Non-Hermitian Evolution with Balanced Gain and Loss: Enhancing Quantum Chaos,” *Phys. Rev. Lett.* **128**, 190402 (2022).
- [27] Apollonas S. Matsoukas-Roubeas, Federico Roccati, Julien Cornelius, Zhenyu Xu, Aurelia Chenu, and Adolfo del Campo, “Non-Hermitian Hamiltonian deformations in quantum mechanics,” *JHEP* **01**, 060 (2023).
- [28] Lucas Sá, Pedro Ribeiro, and Tomaž Prosen, “Complex spacing ratios: A signature of dissipative quantum chaos,” *Phys. Rev. X* **10**, 021019 (2020).
- [29] Jiachen Li, Tomaž Prosen, and Amos Chan, “Spectral Statistics of Non-Hermitian Matrices and Dissipative Quantum Chaos,” *Phys. Rev. Lett.* **127**, 170602 (2021).
- [30] Jiachen Li, Stephen Yan, Tomaž Prosen, and Amos Chan, “Spectral form factor in chaotic, localized, and integrable open quantum many-body systems,” (2024), [arXiv:2405.01641 \[cond-mat.stat-mech\]](https://arxiv.org/abs/2405.01641).
- [31] Giorgio Cipolloni and Nicolo Grometto, “The Dissipative Spectral Form Factor for I.I.D. Matrices,” *J. Statist. Phys.* **191**, 21 (2024).
- [32] Antonio M. García-García, Lucas Sá, and Jacobus J. M. Verbaarschot, “Universality and its limits in non-Hermitian many-body quantum chaos using the Sachdev-Ye-Kitaev model,” *Phys. Rev. D* **107**, 066007 (2023).
- [33] Zhenyu Xu, Aurelia Chenu, Tomaž Prosen, and Adolfo del Campo, “Thermofield dynamics: Quantum Chaos versus Decoherence,” *Phys. Rev. B* **103**, 064309 (2021).
- [34] Yi-Neng Zhou, Tian-Gang Zhou, and Pengfei Zhang, “General properties of the spectral form factor in open quantum systems,” *Front. Phys. (Beijing)* **19**, 31202 (2024).
- [35] Kohei Kawabata, Zhenyu Xiao, Tomi Ohtsuki, and Ryuichi Shindou, “Singular-Value Statistics of Non-Hermitian Random Matrices and Open Quantum Systems,” *PRX Quantum* **4**, 040312 (2023).
- [36] Michael A. Nielsen and Isaac L. Chuang, *Quantum Computation and Quantum Information: 10th Anniversary Edition* (Cambridge University Press, 2010).
- [37] Joshua Feinberg and A. Zee, “Non-hermitian random matrix theory: Method of hermitian reduction,” *Nuclear Physics B* **504**, 579–608 (1997).
- [38] Federico Roccati, Federico Balducci, Ruth Shir, and Aurélie Chenu, “Diagnosing non-Hermitian many-body localization and quantum chaos via singular value decomposition,” *Phys. Rev. B* **109**, L140201 (2024).
- [39] Ryusuke Hamazaki, Kohei Kawabata, and Masahito Ueda, “Non-hermitian many-body localization,” *Phys. Rev. Lett.* **123**, 090603 (2019).
- [40] V. M. Martínez Alvarez, J. E. Barrios Vargas, and L. E. F. Foa Torres, “Non-hermitian robust edge states in one dimension: Anomalous localization and eigenspace condensation at exceptional points,” *Phys. Rev. B* **97**, 121401 (2018).
- [41] Shunyu Yao and Zhong Wang, “Edge states and topological invariants of non-hermitian systems,” *Phys. Rev. Lett.* **121**, 086803 (2018).
- [42] Shu Hamanaka and Kohei Kawabata, “Multifractality of Many-Body Non-Hermitian Skin Effect,” (2024), [arXiv:2401.08304 \[cond-mat.str-el\]](https://arxiv.org/abs/2401.08304).
- [43] Arthur J. Parzygnat, Tadashi Takayanagi, Yusuke Taki, and Zixia Wei, “SVD entanglement entropy,” *JHEP* **12**, 123 (2023).
- [44] Subir Sachdev and Jinwu Ye, “Gapless spin-fluid ground state in a random quantum heisenberg magnet,” *Phys. Rev. Lett.* **70**, 3339–3342 (1993).
- [45] A. Kitaev, “A simple model of quantum holography (part 1) and (part 2),” <https://online.kitp.ucsb.edu/online/joint98/kitaev/>, <https://online.kitp.ucsb.edu/online/entangled15/kitaev2/> (2015), talk given at KITP.
- [46] Juan Maldacena and Douglas Stanford, “Remarks on the Sachdev-Ye-Kitaev model,” *Phys. Rev. D* **94**, 106002 (2016).
- [47] Debanjan Chowdhury, Antoine Georges, Olivier Parcollet, and Subir Sachdev, “Sachdev-Ye-Kitaev models and beyond: Window into non-Fermi liquids,” *Rev. Mod. Phys.* **94**, 035004 (2022).
- [48] Vladimir Rosenhaus, “An introduction to the SYK model,” *J. Phys. A* **52**, 323001 (2019).
- [49] Shenglong Xu, Leonard Susskind, Yuan Su, and Brian Swingle, “A Sparse Model of Quantum Holography,” (2020), [arXiv:2008.02303 \[cond-mat.str-el\]](https://arxiv.org/abs/2008.02303).
- [50] Masaki Tezuka, Onur Oktay, Enrico Rinaldi, Masanori Hanada, and Franco Nori, “Binary-coupling sparse Sachdev-Ye-Kitaev model: An improved model of quantum chaos and holography,” *Phys. Rev. B* **107**, L081103 (2023).
- [51] Takanori Anegawa, Norihiro Iizuka, Arkaprava Mukherjee, Sunil Kumar Sake, and Sandip P. Trivedi, “Sparse random matrices and Gaussian ensembles with varying randomness,” *JHEP* **11**, 234 (2023).
- [52] Elena Cáceres, Anderson Misobuchi, and Rafael Pimentel, “Sparse SYK and traversable wormholes,” *JHEP* **11**, 015 (2021).
- [53] Elena Cáceres, Tyler Guglielmo, Brian Kent, and Anderson Misobuchi, “Out-of-time-order correlators and Lyapunov exponents in sparse SYK,” *JHEP* **11**, 088 (2023).
- [54] Antonio M. García-García, Yiyang Jia, Dario Rosa, and Jacobus J. M. Verbaarschot, “Sparse Sachdev-Ye-Kitaev model, quantum chaos and gravity duals,” *Phys. Rev. D* **103**, 106002 (2021).
- [55] Patrick Orman, Hrant Gharibyan, and John Preskill, “Quantum chaos in the sparse SYK model,” (2024), [arXiv:2403.13884 \[hep-th\]](https://arxiv.org/abs/2403.13884).
- [56] Daniel Jafferis, Alexander Zlokapa, Joseph D. Lykken, David K. Kolchmeyer, Samantha I. Davis, Nikolai Lauk, Hartmut Neven, and Maria Spiropulu, “Traversable wormhole dynamics on a quantum processor,” *Nature* **612**, 51–55 (2022).
- [57] Bryce Kobrin, Thomas Schuster, and Norman Y. Yao, “Comment on ‘Traversable wormhole dynamics on a quantum processor’,” (2023), [arXiv:2302.07897 \[quant-ph\]](https://arxiv.org/abs/2302.07897).
- [58] Luca V. Iliesiu, Márk Mezei, and Gábor Sárosi, “The volume of the black hole interior at late times,” *JHEP* **07**, 073 (2022).
- [59] Antonio M. García-García and Victor Godet, “Euclidean wormhole in the Sachdev-Ye-Kitaev model,” *Phys. Rev. D* **103**, 046014 (2021).
- [60] Antonio M. García-García, Lucas Sá, and Jacobus J. M. Verbaarschot, “Symmetry Classification and Universal-

- ity in Non-Hermitian Many-Body Quantum Chaos by the Sachdev-Ye-Kitaev Model,” *Phys. Rev. X* **12**, 021040 (2022).
- [61] Antonio M. García-García, Yiyang Jia, Dario Rosa, and Jacobus J. M. Verbaarschot, “Replica symmetry breaking in random non-Hermitian systems,” *Phys. Rev. D* **105**, 126027 (2022).
- [62] Giorgio Cipolloni and Jonah Kudler-Flam, “Entanglement Entropy of Non-Hermitian Eigenstates and the Ginibre Ensemble,” *Phys. Rev. Lett.* **130**, 010401 (2023).
- [63] Shashi C L Srivastava, Arul Lakshminarayanan, Steven Tomsovic, and Arnd Bäcker, “Ordered level spacing probability densities,” *Journal of Physics A: Mathematical and Theoretical* **52**, 025101 (2018).
- [64] Matthias Allard and Mario Kieburg, “Correlation functions between singular values and eigenvalues,” (2024), [arXiv:2403.19157 \[math.PR\]](https://arxiv.org/abs/2403.19157).
- [65] Dorje C Brody, “Biorthogonal quantum mechanics,” *Journal of Physics A: Mathematical and Theoretical* **47**, 035305 (2013).
- [66] Eiki Iyoda, Hosho Katsura, and Takahiro Sagawa, “Effective dimension, level statistics, and integrability of Sachdev-Ye-Kitaev-like models,” *Phys. Rev. D* **98**, 086020 (2018).
- [67] Lucas Sá and Antonio M. García-García, “Q-Laguerre spectral density and quantum chaos in the Wishart-Sachdev-Ye-Kitaev model,” *Phys. Rev. D* **105**, 026005 (2022).
- [68] Yi-Zhuang You, Andreas W. W. Ludwig, and Cenke Xu, “Sachdev-Ye-Kitaev Model and Thermalization on the Boundary of Many-Body Localized Fermionic Symmetry Protected Topological States,” *Phys. Rev. B* **95**, 115150 (2017).
- [69] R. E. Prange, “The spectral form factor is not self-averaging,” *Phys. Rev. Lett.* **78**, 2280–2283 (1997).
- [70] Pak Hang Chris Lau, Chen-Te Ma, Jeff Murugan, and Masaki Tezuka, “Correlated disorder in the SYK₂ model,” *J. Phys. A* **54**, 095401 (2021).
- [71] Soshun Ozaki and Hosho Katsura, “Disorder-Free Sachdev-Ye-Kitaev models: Integrability and Quantum Chaos,” (2024), [arXiv:2402.13154 \[cond-mat.str-el\]](https://arxiv.org/abs/2402.13154).
- [72] Hrant Gharibyan, Masanori Hanada, Stephen H. Shenker, and Masaki Tezuka, “Onset of Random Matrix Behavior in Scrambling Systems,” *JHEP* **07**, 124 (2018), [Erratum: *JHEP* **02**, 197 (2019)].
- [73] Tomoki Nosaka, Dario Rosa, and Junggi Yoon, “The Thouless time for mass-deformed SYK,” *JHEP* **09**, 041 (2018).
- [74] D. J. Thouless, “Maximum metallic resistance in thin wires,” *Phys. Rev. Lett.* **39**, 1167–1169 (1977).
- [75] László Erdős and Antti Knowles, “The Altshuler–Shklovskii Formulas for Random Band Matrices I: the Unimodular Case,” *Communications in Mathematical Physics* **333**, 1365–1416 (2015).
- [76] Apollonas S. Matsoukas-Roubeas, Mathieu Beau, Lea F. Santos, and Adolfo del Campo, “Unitarity breaking in self-averaging spectral form factors,” *Phys. Rev. A* **108**, 062201 (2023).
- [77] Olivier Giraud, Nicolas Macé, Éric Vernier, and Fabien Alet, “Probing Symmetries of Quantum Many-Body Systems through Gap Ratio Statistics,” *Phys. Rev. X* **12**, 011006 (2022).
- [78] Juan Martin Maldacena, “The Large N limit of superconformal field theories and supergravity,” *Adv. Theor. Math. Phys.* **2**, 231–252 (1998).
- [79] Edward Witten, “Anti-de Sitter space and holography,” *Adv. Theor. Math. Phys.* **2**, 253–291 (1998).
- [80] Ro Jefferson and Robert C. Myers, “Circuit complexity in quantum field theory,” *JHEP* **10**, 107 (2017).
- [81] Johanna Erdmenger, Shao-Kai Jian, and Zhuo-Yu Xian, “Universal chaotic dynamics from Krylov space,” *JHEP* **08**, 176 (2023).
- [82] Hugo A. Camargo, Viktor Jahnke, Hyun-Sik Jeong, Keun-Young Kim, and Mitsuhiro Nishida, “Spectral and Krylov complexity in billiard systems,” *Phys. Rev. D* **109**, 046017 (2024).
- [83] Hugo A. Camargo, Kyoung-Bum Huh, Viktor Jahnke, Hyun-Sik Jeong, Keun-Young Kim, and Mitsuhiro Nishida, “Spread and Spectral Complexity in Quantum Spin Chains: from Integrability to Chaos,” (2024), [arXiv:2405.11254 \[hep-th\]](https://arxiv.org/abs/2405.11254).
- [84] Vijay Balasubramanian, Pawel Caputa, Javier M. Magan, and Qingyue Wu, “Quantum chaos and the complexity of spread of states,” *Phys. Rev. D* **106**, 046007 (2022).
- [85] Daniel E. Parker, Xiangyu Cao, Alexander Avdoshkin, Thomas Scaffidi, and Ehud Altman, “A Universal Operator Growth Hypothesis,” *Phys. Rev. X* **9**, 041017 (2019).
- [86] Antonio M. García-García, Lucas Sá, Jacobus J. M. Verbaarschot, and Jie Ping Zheng, “Keldysh wormholes and anomalous relaxation in the dissipative Sachdev-Ye-Kitaev model,” *Phys. Rev. D* **107**, 106006 (2023).
- [87] Wenhe Cai, Sizheng Cao, Xian-Hui Ge, Masataka Matsumoto, and Sang-Jin Sin, “Non-Hermitian quantum system generated from two coupled Sachdev-Ye-Kitaev models,” *Phys. Rev. D* **106**, 106010 (2022).
- [88] Antonio M. García-García, Bruno Loureiro, Aurelio Romero-Bermúdez, and Masaki Tezuka, “Chaotic-Integrable Transition in the Sachdev-Ye-Kitaev Model,” *Phys. Rev. Lett.* **120**, 241603 (2018).
- [89] S. Harshini Tekur, Udaysinh T. Bhosale, and M. S. Senthnam, “Higher-order spacing ratios in random matrix theory and complex quantum systems,” *Phys. Rev. B* **98**, 104305 (2018).
- [90] Ferdinand Evers and Alexander D. Mirlin, “Anderson transitions,” *Rev. Mod. Phys.* **80**, 1355–1417 (2008).
- [91] Antonio M. García-García and Jacobus J. M. Verbaarschot, “Spectral and thermodynamic properties of the Sachdev-Ye-Kitaev model,” *Phys. Rev. D* **94**, 126010 (2016).